

# Self-oscillation and Synchronisation Transitions in Elasto-Active Structures

Ellen Zheng,<sup>1</sup> Martin Brandenbourger,<sup>1</sup> Louis Robinet,<sup>1</sup> Peter Schall,<sup>1</sup> Edan Lerner,<sup>1</sup> and Corentin Coulais<sup>1</sup>

<sup>1</sup>*Institute of Physics, Universiteit van Amsterdam,  
Science Park 904, 1098 XH Amsterdam, The Netherlands*

The interplay between activity and elasticity often found in active and living systems triggers a plethora of autonomous behaviors ranging from self-assembly and collective motion to actuation. Amongst these, spontaneous self-oscillations of mechanical structures is perhaps the simplest and most wide-spread type of non-equilibrium phenomenon. Yet, we lack experimental model systems to investigate the various dynamical phenomena that may appear. Here, we introduce a centimeter-sized model system for one-dimensional elasto-active structures. We show that such structures exhibit flagellar motion when pinned at one end, self-snapping when pinned at two ends, and synchronization when coupled together with a sufficiently stiff link. We further demonstrate that these transitions can be described quantitatively by simple models of coupled pendula with follower forces. Beyond the canonical case considered here, we anticipate our work to open avenues for the understanding and design of the self-organisation and response of active biological and synthetic solids, e.g. in higher dimensions and for more intricate geometries.

*Introduction.* — Active matter systems exhibit exceptional collective, non-equilibrium properties resulting in anomalous dynamical and self-organizing behaviours that challenge conventional laws of statistical mechanics [1–10]. While researches have extensively focused on active fluids [2, 11]—which consist of collections of individual active particles with no particular geometry [12–16], active solids—which have a well defined reference state and hence exhibit elastic rather than viscous properties at long timescales [17–19]—have been much less studied, despite their potential in mimicking living matter and forming novel active materials [18–20].

Among all kinds of mechanical properties of active solids, self-oscillations are vital for biological systems such as flagella and cilia [21–23] and offer the prospect of autonomous mechanical behaviors in designer materials [18, 19, 24]. It is now well established that one-dimensional active chains exhibit flagellar motion: on the one hand, experimental studies have reported self-oscillatory behavior and synchronization in biological and colloidal systems [25–30]; on the other hand, theoretical and numerical studies have suggested that self-oscillations emerge from the competition between activity and elasticity [21–23, 26, 31–43]. Despite these advances, there are as of yet few model experimental platforms in which the predicted bifurcation scenarios that lead to self-oscillations and synchronization can be verified.

Here, to investigate dynamical transitions in elasto-active solids, we construct the experimental setup for a simplest form of active solids by elastically constraining centimeter-sized active particles in one-dimensional chains that can freely oscillate in the 2d plane. By controlling the elasticity of such structures, we uncover the nature of the transition to self-oscillations and synchronization. We find the transition to flagellar and self-snapping motion is governed by a nonlinear feedback between the direction of the active forces and the nonlinear

elastic deflections. We find that synchronization between two elasto-active chains is mediated by elastically driven alignment, in contrast with active fluids. Although our proposed experimental platform is macroscopic, it might nonetheless help to advance our understanding of elasto-active instabilities that occur at the smaller scale in bi-

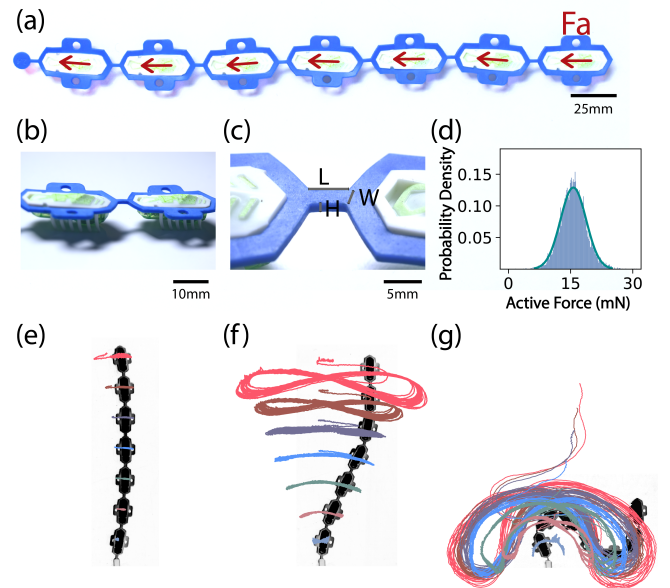


FIG. 1. Emergence of Self Oscillations in elasto-active chains. (a) Configurations of 7 active particles connected by a flexible rubber chain (b) zoomed in details of two active particles unveiling the design of the microbot (c) a close-up of the linkage between each particle with width ( $W$ ), thickness ( $H$ ) and length ( $L$ ). (d) Histogram of the active force measurements conducted at 0.05 mm/min. (e)-(f) Snapshots of the trajectories of the active particles showing the oscillations changed from self-amplified to overdamped with  $W = 5$  mm, 4.4mm and 2mm corresponding to elasto-active number  $\sigma = 0.17$ , 0.21 and 0.80 respectively. See also Supplementary Videos.

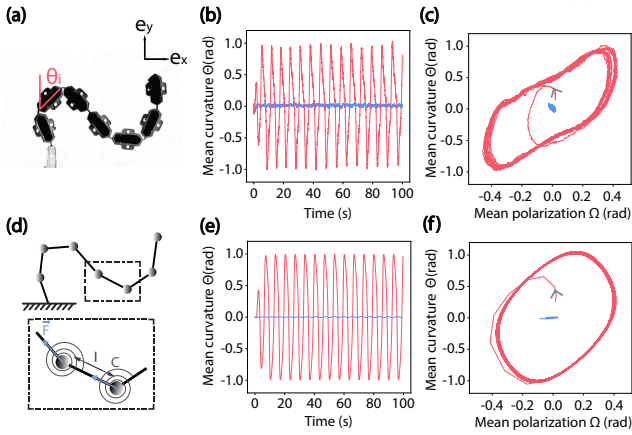


FIG. 2. Characterisation of the dynamics of elasto-active chains. (a) Snapshot of the elasto-active chain with  $W=17.7\text{mm}$  during its self-oscillation. (b) Time series of the angle between the first and last particle (mean polarisation) was one of the parameters we chose to characterize the system, blue and orange represent the  $\sigma = 0.695$  and  $\sigma = 0.166$  chain respectively. With the average of tangential angles of the particles (mean curvature) being the other parameter, plotting mean polarisation ( $\Theta$ ) against mean curvature ( $\Omega$ ) gives (c) limit cycle showing that active forces balance with dissipation towards stable self-oscillation. (d) Schematics of an elasto-active chain of 7 pendulums with active forces. (e)-(f) Simulation results at  $\sigma=0.8$  showing good agreement with the experimental results.

ological solids. We further envision that it will provide design guidelines for autonomous behaviors in active solids [44, 45].

*Experimental design of active chains.* — Our system consists of  $N = 7$  5cm commercial self-propelled microbots (Hexbug Nano v2) [8, 46] elastically coupled by a laser-cut silicon rubber chain pinned at one end as shown in FIG.1(a,b)[47]. By tuning the width of the connection ( $W$  in FIG.1(c)), we are able to manipulate the stiffness of the chain. When constrained at zero velocity, the microbot exerts a force in the direction of its polarisation which is parallel to the chain’s axis at rest and point in the same direction, towards the anchor point of the chain (FIG.1(d)).

*Transition to self-oscillations.* — The chain with the largest width in between the active particles was slightly pushed off from the equilibrium and stayed at the same position without further significant movements as shown in FIG.1 (e). We then gradually reduced the width of the connections, at  $W = 4.25 \pm 0.1\text{mm}$ , the self-oscillation behaviour started to emerge (FIG.1 (f)) suggesting a competition between activity and elasticity: Active forces from active particles destabilise the elastic chain, which in turn, through deformation, re-orient the polarisation of the particle, ultimately leading to self-oscillation. The magnitude of the oscillations increases drastically (shown

in FIG.1 (g)) with decreasing  $W$  thanks to the competition between buckling and active force. This oscillatory dynamics can be quantified by the mean curvature  $\Theta(t) := \sum_{i=1}^{N-1} \theta_{i+1}(t) - \theta_i(t) = \theta_7 - \theta_1$  and the mean polarization  $\Omega(t) := \frac{1}{N} \sum_{i=1}^N \theta_i(t)$ , where  $\theta_i(t)$  is the instantaneous orientation of particle  $i$  w.r.t. the vertical axis (FIG.2 (a,b)). While chains with large  $W$  come to a standstill, softer chains exhibit a limit cycle (FIG.2 (c)). The area of this limit cycle arises directly from a balance of energy injection with dissipation.

*Active pendulums model.* — What is the origin of such transition? Inspired by the Ziegler destabilisation paradox in structural mechanics [48–51] and the existing numerical models of active filaments [52–55], we construct a discrete model, where we boil the complexity of the elastic interactions down to three-body bending forces between the particles and the complexity of the vibration-induced dynamics to viscous overdamped dynamics. The discrete model is based on a chain of seven pendulums (shown as FIG.2(d)) with one end fixed. The pendulums have a length  $\ell$  and are connected to their neighbors via a torsional spring of torsional stiffness  $C$ . Each pendulum  $i$  is driven by a constant active force  $\mathbf{F}_i^a = -F^a(\cos \theta_i \mathbf{e}_x + \sin \theta_i \mathbf{e}_y)$  exerted on its end and in the direction of the pendulum. We also introduce isotropic viscosity  $\gamma$  contributing to a dissipative force on the end of each pendulum that is only dependent on its velocity, and assume no inertia in the system [56]. We then collected all the terms in  $\delta\theta_i$  for each  $i$  according to Virtual-Work Theorem and constructed  $N$  nonlinear coupled DAEs that describe the motion of the elasto-active chain (further details in SI). There  $\sigma = F^a \ell / C$  is the elasto-active parameter and  $\tau = \gamma \ell^2 / C$  a characteristic timescale. We estimate the torsional stiffness  $C$  from their geometry using beam theory (See Appendix A). From the average velocity of the robots when they are freely moving  $v_a = 0.025 \pm 0.005\text{m/s}$  and their average force when they are pinned  $F_a = 15.7 \pm 3.1\text{mN}$  (Fig. 1(d)), we estimate the damping coefficient  $\gamma = F_a / v_a = 0.63 \pm 0.11\text{N.s/m}$ .

Using these parameters, we solve the system of DAEs numerically (See SI) and find a good agreement with the experimental results, and for the time series of average polarisation (Fig. 2(e)). We observe an agreement between the experiments and the simulation in the trend of the limit cycle (Fig. 2(f)), here the differences are due to the energy loss in the experimental scenarios. This agreement shows that nonlinear geometry, torsional stiffness, active force and isotropic viscous dissipation are sufficient ingredients to successfully capture the essence of the self-oscillation phenomenon. The critical elasto-active number decreases with the length of the chain as  $\sim 1/N^3$ , See SI[57] for simulations and theory, this can be interpreted by two effects: the Euler buckling load decreases for longer chains  $\sim 1/N^2$  while the sum of the active forces grows as  $N$ . Our elasto-active model is controlled

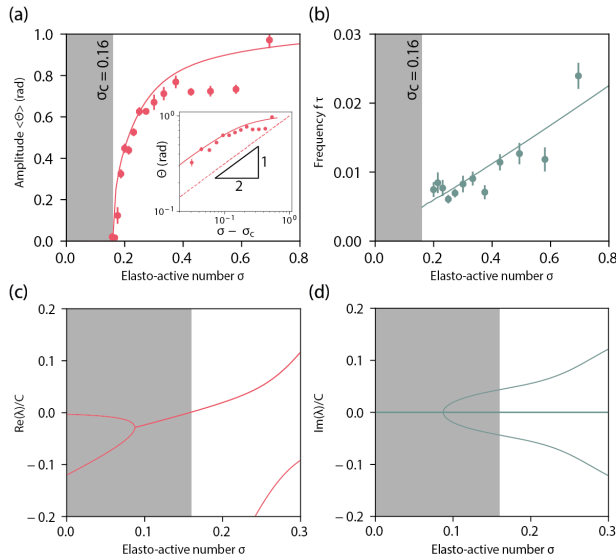


FIG. 3. An active system featuring a Hopf bifurcation at  $\sigma = 0.15$ . Simulation and experimental results showing the evolution of (a) amplitude and (b) frequency with increasing  $\sigma$  respectively for the chain with  $N = 7$ . The inset in (a) is a log-log plot demonstrating the power law between  $\Theta$  and  $\sigma$ . (c) Real and imaginary (d) part of the eigenvalues of the Jacobian of Eqs. (1)-(2) vs. elasto-active number  $\sigma$  for a minimal chain with  $N = 2$ . In all panels, the gray area represents the stable region.

by a single timescale  $\tau$  and a single non-dimensional parameter  $\sigma$ , which will allow us to probe the nature of the transition to self-oscillations in the following.

*Super-critical Hopf bifurcation.* — We ran experiments and simulations over a wide range of the elasto-active parameter  $\sigma$ , collected the time average of the amplitudes  $\langle \Theta \rangle$  (Fig. 3 (a)) and the rescaled oscillation frequency  $f \times \tau$  (Fig. 3 (b)) in the mean polarisation time series and plotted them against elasto-active parameter  $\sigma$ . While for low values of  $\sigma$ , the chain remains straight without oscillations, we see that above a critical value  $\sigma_c = 0.16 \pm 0.005$ , the oscillation amplitude  $\langle \Theta \rangle$  increases rapidly as  $\langle \Theta \rangle \sim (\sigma - \sigma_c)^{0.5}$  (Fig. 3 (a-inset)), while the rescaled frequency increases linearly. To further elucidate the nature of the transition to self-oscillations, we carry out a linear stability analysis on the set of nonlinear coupled equations (See SI), and observe that at  $\sigma = 0.15$ , the real part of a pair of eigenvalues becomes positive, while the corresponding imaginary parts of these eigenvalues are equal and opposite and monotonically increase (Fig. 3(cd)). This transition is a hallmark of a Hopf-bifurcation. The exponent 0.5 in the experimental and numerical data suggests that this bifurcation is supercritical. To verify the nature of the bifurcation theoretically, we restrict our attention to two pendulums with  $N = 2$ , which is the simplest case where the model could exhibit

the bifurcation. The time-evolution of such elasto-active chain is governed by the following equations

$$\tau \left( 2\dot{\theta}_1 + \dot{\theta}_2 \cos(\theta_1 - \theta_2) \right) = \theta_2 - 2\theta_1 + \sigma \sin(\theta_1 - \theta_2) \quad (1)$$

$$\tau \left( \dot{\theta}_1 \cos(\theta_1 - \theta_2) + \dot{\theta}_2 \right) = \theta_1 - \theta_2. \quad (2)$$

In SI, we use a perturbative expansion and perform a few algebraic manipulations to demonstrate that Eqs. (1-2) can be mapped onto the Landau-Stuart equation

$$\frac{dz}{dt} = (i + \sigma - 3)z + \left( i \left( \frac{17}{4} - \sigma \right) - \left( \sigma - \frac{5}{2} \right) \right) |z|^2 z, \quad (3)$$

where  $z$  is the complex variable defined by  $z := \theta_1 + i\sqrt{(\sigma - 2)/(4 - \sigma)}\theta_2$ . This equation is the canonical form of a supercritical Hopf-bifurcation. Many earlier works had observed experimentally or numerically self-oscillation phenomena [21, 25, 58] or theoretically proposed models with Hopf-bifurcations [23, 31, 32, 35, 55, 59]; here, we unambiguously demonstrate experimentally, numerically and theoretically in a single system of active chains that the supercritical Hopf bifurcation underlies the transition to self-oscillations and is primarily controlled by the elasto-active number  $\sigma$ .

*Self-snapping.* — When experimenting with the elasto-active chain, we realized that not only does it oscillate when pinned at one end, it also does oscillate when pinned at two ends, Fig. 4a. We find that these oscillations vanish when the chain is maintained at its undeformed length, but that they immediately emerge once we compress the chain along its axis. A passive chain would simply buckle, i.e. bend sideways when compressed. In stark contrast, the elasto-active chain bends sideways, but continuously snaps by itself from one side to the other. The more the chain is compressed, the more it oscillates (Fig. 4c) and the slower it self-snaps (Fig. 4d). We find that adding geometrical constraints to our model (See SI) allows us to reproduce the phenomenology qualitatively (Fig. 4b) [60]. While the flagellar motion observed earlier is ubiquitous in the context of biological structures, this self-snapping oscillation of buckled elasto-active structures is much more rare and surprising.

*Frequency entrainment synchronisation transition.* — Our model system also allows us to explore synchronisation phenomena between two active chains (FIG.5 (a)-(d)). We demonstrate experimentally and numerically that an elastic coupling allows for a frequency entrainment synchronization transition. We selected two chains both with an elasto-active number  $\sigma_1 = 0.8$  (the chain on the left hand side in FIG 5 (a)) and an elasto-active number  $\sigma_2 = 0.6$  (the chain on the right hand side in FIG 5 (a)) and connected them via a coupling spring of variable stiffness  $K$ . We also performed simulations over a range of stiffness  $K$  that contains what we have utilised in the experiments (FIG.5 (e)-(f)). The rescaled coupling stiffness is  $\kappa := K\ell^2/C_1$  (where  $C_1$  is the stiffness of the left

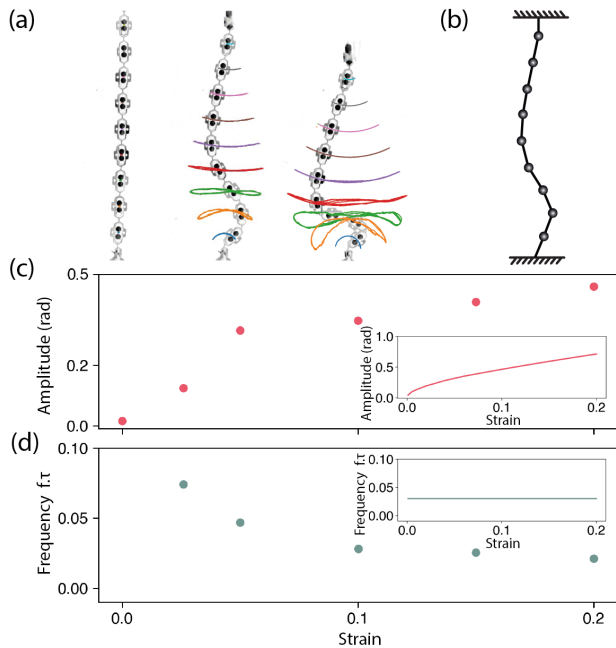


FIG. 4. **Elasto-active chains pinned at both ends.** Stills of an active chain where both ends are pinned with overlaid trajectories of the hexbugs. The end-to-end distance between the pinning points is  $\ell = 500$  mm (left),  $\ell = 475$  mm (middle) and  $\ell = 400$  mm (right). The length of the undeformed chain is  $L = 500$  mm. (b) Model: sketch of the chain pinned at both ends. (c) Amplitude and (d) frequency of the self-snapping oscillations vs. the compressive strain  $(L - \ell)/L$ . The inset are the corresponding data from the numerical model defined in the SI. The elasto-active number of the chain is  $\sigma = 0.8$ . See also Supplementary Videos.

chain). To analyze the synchronization transition, we first extracted the oscillation signals from both chains. We then calculated the instantaneous phases  $\Phi_1(t)$  and  $\Phi_2(t)$  (see Appendix A) of each timeseries (Fig. 5(b) and (e)) for experiments and simulations respectively). For low coupling stiffness (yellow lines), both  $\Phi_1(t)$  and  $\Phi_2(t)$  increase linearly, but with different slope, which can be described as two chains oscillating with different frequencies. On the contrary, for large coupling stiffness (brown lines), both instantaneous phases  $\Phi_1(t)$  and  $\Phi_2(t)$  align on the lowest slope (i.e. both chains beat at the lowest frequency of the two). We performed experiments and numerical simulations and measured the frequency mismatch  $\delta\nu$  from the slope of the instantaneous phase difference  $\Psi := \Phi_2(t) - \Phi_1(t)$  over a wide range of coupling stiffness and found that the synchronization transition occurs at the critical value  $\kappa = 1.1$  (Fig. 5(c) and (f)) [61]. Further numerical simulations of elasto-active chains with varying  $\sigma$  reveal that the regime of synchronization exhibits an Arnold tongue centered about the 1:1 frequency ratio in the synchronization regime (Fig. 5 (f) inset). In other words, the two chains will synchronize for

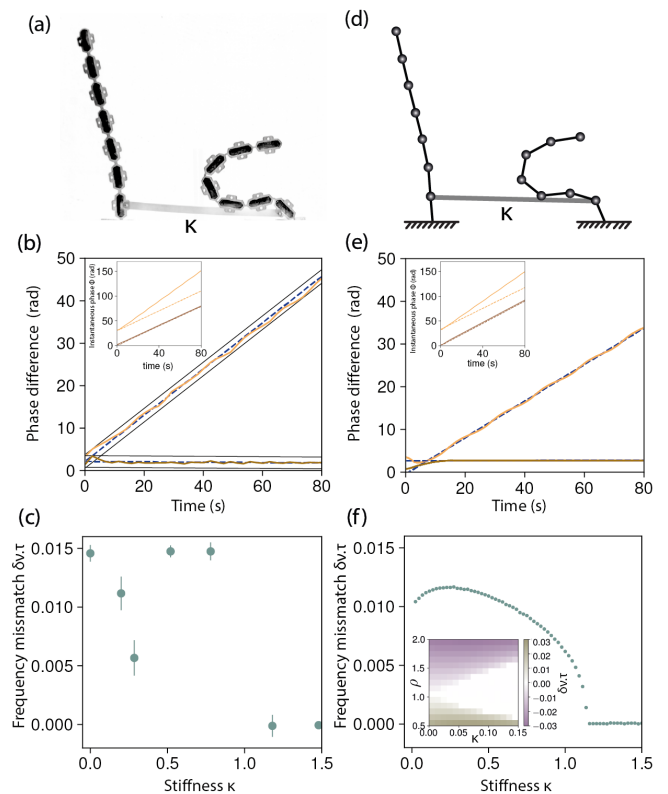


FIG. 5. **Synchronisation of two elasto-active chains with different elasticity coupled by the first particles only.** (a) Snapshot of a pair of elasto-active chains with different elasticity coupled by another stiff silicon rubber chain. (b) Evolution of the instantaneous phase differences (instantaneous phases  $\Phi_1$  (dashed lines) and  $\Phi_2$  (solid lines) in inset) of two elasto-active chains with coupling strength  $K = 0.8$  (yellow lines) and  $K = 1.2$  (brown lines). (c) Instantaneous frequency difference extracted from the instantaneous phase difference  $\Psi$  vs. rescaled coupling stiffness  $\kappa$ , with error bars corresponding to deviations on the linear regression (dashed blue line and black lines in panel b). (d) Schematics of the numerical model adding a coupling spring ( $K$ ) to two previously established elasto-active chains. (e)-(f) Same data as (b)-(c) for the numerical simulations. An Arnold tongue is observed when the frequency miss-match is plotted against the ratio between both elasto-active numbers  $\rho$  and the stiffness  $\kappa$  (inset of panel f).

lower coupling if they have similar elasto-active numbers or if they are closer to the bifurcation—in this case the transition towards steady oscillatory synchronized state will take longer.

To rationalize this finding, we show in SI that the instantaneous phase difference  $\Psi(t)$  between two chains with  $N = 2$  is

$$\frac{d\Psi}{dt} = d\nu - \frac{\varepsilon}{\cos\Psi_0} \sin(\Psi - \Psi_0), \quad (4)$$

where  $d\nu$ ,  $\varepsilon$  and  $\Psi_0$  are functions of the elasto-active

number of each chain and of the coupling stiffness between the chains (See SI for closed forms). This equation has been well studied before for the investigation of synchronization phenomena [62]. An analysis of this equation predicts synchronization for  $|\varepsilon/\cos\psi_0| > |d\nu|$ , with a square root singularity [62]. As we show in the appendix, this condition is met when the coupling stiffness exceeds the threshold value  $\kappa_c = 11/(4\sqrt{6})\sqrt{(\sigma-3)|1-\rho|}$ , where  $\sigma$  is the elasto-active number of the left chain and where  $\rho$  is ratio between the elasto-active number of the right chain over that of the left chain. This result thus demonstrates that the synchronization scenario of the two elasto-active chains corresponds to that of a classic nonisochronous synchronization, which is characterized by a constant phase shift in the synchronized region. In addition, the two chains will synchronize for lower coupling if they are closer to the bifurcation or when they have similar elasto-active numbers. In summary, we have captured experimentally, numerically and analytically the synchronization transition of two elastically coupled active chains.

*Conclusion.* — In conclusion, we have shown that elasto-active chains exhibit transitions to self-oscillations and synchronization. Since they exhibit a nonlinear dynamics that is governed by activity, elasticity and viscous damping, our study establishes macroscopic active structures as a powerful tool to investigate dynamical and autonomous behavior of active solids and living matter that exhibit collective self-oscillation at the microscale. Finally, fascinating future research directions could be taken from the minimalistic system considered here. For instance, one could investigate more complex geometries, such as non-follower forces [44], more intricate geometrical connections between active particles, two-dimensional structures, alternative boundary conditions—pinned or moving clamping points (See Appendix A)—or even mechanical responses such as longitudinal or transverse excitations. These could in particular emulate peculiar dynamics observed in other contexts, such as odd elasticity [19] or the non-Hermitian skin effect [18, 63].

*Acknowledgments.* — We thank D. Giesen, S. Koot and all the staff members from the Technology Centre of University of Amsterdam for their technical support. We acknowledge K. Sekimoto, A. Deblais, R. Sinaasappel, D. Tam and M. Jalaal for insightful discussions. We acknowledge funding from the Netherlands Organization for Scientific Research through support from the NWO (Vidi grant no. 680-47-554/3259) and from the European Research Council Starting Grant No. ERC-StG-Coulais-852587-Extr3Me (C.C.). The data and codes supporting this study are publicly available on Zenodo at <https://doi.org/10.5281/zenodo.6549887>.

- 
- [1] Suropriya Saha, Ramin Golestanian, and Sriram Ramaswamy, “Clusters, asters, and collective oscillations in chemotactic colloids,” *Phys. Rev. E* **89**, 062316 (2014).
  - [2] M. C. Marchetti, J. F. Joanny, S. Ramaswamy, T. B. Liverpool, J. Prost, Madan Rao, and R. Aditi Simha, “Hydrodynamics of soft active matter,” *Rev. Mod. Phys.* **85**, 1143–1189 (2013).
  - [3] Sriram Ramaswamy, “Active matter,” *Journal of Statistical Mechanics: Theory and Experiment* **2017**, 054002 (2017).
  - [4] Clemens Bechinger, Roberto Di Leonardo, Hartmut Löwen, Charles Reichardt, Giorgio Volpe, and Giovanni Volpe, “Active particles in complex and crowded environments,” *Rev. Mod. Phys.* **88**, 045006 (2016).
  - [5] J. Deseigne, O. Dauchot, and H. Chate, “Collective motion of vibrated polar disks,” *Phys Rev Lett* **105**, 098001 (2010).
  - [6] C. A. Weber, T. Hanke, J. Deseigne, S. Léonard, O. Dauchot, E. Frey, and H. Chaté, “Long-range ordering of vibrated polar disks,” *Phys. Rev. Lett.* **110**, 208001 (2013).
  - [7] Antoine Bricard, Jean-Baptiste Caussin, Nicolas Desreumaux, Olivier Dauchot, and Denis Bartolo, “Emergence of macroscopic directed motion in populations of motile colloids,” *Nature* **503**, 95 (2013).
  - [8] O. Dauchot and V. Demery, “Dynamics of a self-propelled particle in a harmonic trap,” *Phys Rev Lett* **122**, 068002 (2019).
  - [9] Tamás Vicsek and Anna Zafeiris, “Collective motion,” *Physics Reports* **517**, 71 – 140 (2012), collective motion.
  - [10] Aparna Baskaran and M Cristina Marchetti, “Statistical mechanics and hydrodynamics of bacterial suspensions,” *Proceedings of the National Academy of Sciences* **106**, 15567–15572 (2009).
  - [11] David Saintillan and Michael J Shelley, “Active suspensions and their nonlinear models,” *Comptes Rendus Physique* **14**, 497–517 (2013).
  - [12] Peter Reimann, “Brownian motors: noisy transport far from equilibrium,” *Physics Reports* **361**, 57 – 265 (2002).
  - [13] Walter F Paxton, Kevin C Kistler, Christine C Olmeda, Ayusman Sen, Sarah K St. Angelo, Yanyan Cao, Thomas E Mallouk, Paul E Lammert, and Vincent H Crespi, “Catalytic nanomotors: autonomous movement of striped nanorods,” *Journal of the American Chemical Society* **126**, 13424–13431 (2004).
  - [14] Jonathan R Howse, Richard AL Jones, Anthony J Ryan, Tim Gough, Reza Vafabakhsh, and Ramin Golestanian, “Self-motile colloidal particles: from directed propulsion to random walk,” *Physical review letters* **99**, 048102 (2007).
  - [15] Eric Lauga and Thomas R Powers, “The hydrodynamics of swimming microorganisms,” *Reports on Progress in Physics* **72**, 096601 (2009).
  - [16] WCK Poon, “From clarkia to escherichia and janus: The physics of natural and synthetic active colloids,” *Proc. Int. Sch. Phys. Enrico Fermi* **184**, 317–386 (2013).
  - [17] Rhoda J Hawkins and Tanniemola B Liverpool, “Stress reorganization and response in active solids,” *Physical review letters* **113**, 028102 (2014).
  - [18] M. Brandenbourger, X. Locsin, E. Lerner, and C. Coulais, “Non-reciprocal robotic metamaterials,” *Nat Commun* **10**, 4608 (2019).

- [19] Colin Scheibner, Anton Souslov, Debarghya Banerjee, Piotr Surówka, William T. M. Irvine, and Vincenzo Vitelli, “Odd elasticity,” *Nat. Phys.* **16**, 475–480 (2020).
- [20] Y. Ozkan-Aydin, D. I. Goldman, and M. S. Bhamla, “Collective dynamics in entangled worm and robot blobs,” *Proc Natl Acad Sci U S A* **118** (2021), 10.1073/pnas.2010542118.
- [21] KE Machin, “Wave propagation along flagella,” *Journal of Experimental Biology* **35**, 796–806 (1958).
- [22] Charles J Brokaw, “Molecular mechanism for oscillation in flagella and muscle,” *Proceedings of the National Academy of Sciences* **72**, 3102–3106 (1975).
- [23] Sébastien Camalet, Frank Jülicher, and Jacques Prost, “Self-organized beating and swimming of internally driven filaments,” *Physical review letters* **82**, 1590 (1999).
- [24] F. G. Woodhouse, H. Ronellenfitsch, and J. Dunkel, “Autonomous actuation of zero modes in mechanical networks far from equilibrium,” *Phys Rev Lett* **121**, 178001 (2018).
- [25] Daiki Nishiguchi, Junichiro Iwasawa, Hong-Ren Jiang, and Masaki Sano, “Flagellar dynamics of chains of active janus particles fueled by an ac electric field,” *New Journal of Physics* **20**, 015002 (2018).
- [26] Kirsty Y Wan, Kyriacos C Leptos, and Raymond E Goldstein, “Lag, lock, sync, slip: the many ‘phases’ of coupled flagella,” *Journal of the Royal Society Interface* **11**, 20131160 (2014).
- [27] Wei Zhou, Zhuonan Hao, and Nick Gravish, “Collective synchronization of undulatory movement through contact,” *Phys. Rev. X* **11**, 031051 (2021).
- [28] Douglas R Brumley, Kirsty Y Wan, Marco Polin, and Raymond E Goldstein, “Flagellar synchronization through direct hydrodynamic interactions,” *Elife* **3**, e02750 (2014).
- [29] Raymond E Goldstein, Marco Polin, and Idan Tuval, “Emergence of synchronized beating during the regrowth of eukaryotic flagella,” *Physical Review Letters* **107**, 148103 (2011).
- [30] Raj Kumar Manna, PB Sunil Kumar, and R Adhikari, “Colloidal transport by active filaments,” *The Journal of Chemical Physics* **146**, 024901 (2017).
- [31] A Hilfinger and F Jülicher, “The chirality of ciliary beats,” *Physical biology* **5**, 016003 (2008).
- [32] Andreas Hilfinger, Amit K Chattopadhyay, and Frank Jülicher, “Nonlinear dynamics of cilia and flagella,” *Physical Review E* **79**, 051918 (2009).
- [33] Henry C Fu, Charles W Wolgemuth, and Thomas R Powers, “Beating patterns of filaments in viscoelastic fluids,” *Physical Review E* **78**, 041913 (2008).
- [34] Jannes Gladrow, Chase P Broedersz, and Christoph F Schmidt, “Nonequilibrium dynamics of probe filaments in actin-myosin networks,” *Physical Review E* **96**, 022408 (2017).
- [35] Raghunath Chelakkot, Arvind Gopinath, Lakshminarayanan Mahadevan, and Michael F Hagan, “Flagellar dynamics of a connected chain of active, polar, brownian particles,” *Journal of The Royal Society Interface* **11**, 20130884 (2014).
- [36] Greta Quaranta, Marie-Eve Aubin-Tam, and Daniel Tam, “Hydrodynamics versus intracellular coupling in the synchronization of eukaryotic flagella,” *Physical review letters* **115**, 238101 (2015).
- [37] Kirsty Y Wan and Raymond E Goldstein, “Coordinated beating of algal flagella is mediated by basal coupling,” *Proceedings of the National Academy of Sciences* **113**, E2784–E2793 (2016).
- [38] Thomas Niedermayer, Bruno Eckhardt, and Peter Lenz, “Synchronization, phase locking, and metachronal wave formation in ciliary chains,” *Chaos: An Interdisciplinary Journal of Nonlinear Science* **18**, 037128 (2008).
- [39] Boris Guirao and Jean-François Joanny, “Spontaneous creation of macroscopic flow and metachronal waves in an array of cilia,” *Biophysical journal* **92**, 1900–1917 (2007).
- [40] Gayathri Jayaraman, Sanoop Ramachandran, Somdeb Ghose, Abhrajit Laskar, M Saad Bhamla, PB Sunil Kumar, and R Adhikari, “Autonomous motility of active filaments due to spontaneous flow-symmetry breaking,” *Physical review letters* **109**, 158302 (2012).
- [41] Rachel R Bennett and Ramin Golestanian, “Emergent run-and-tumble behavior in a simple model of chlamydomonas with intrinsic noise,” *Physical review letters* **110**, 148102 (2013).
- [42] Andrej Vilfan and Frank Jülicher, “Hydrodynamic flow patterns and synchronization of beating cilia,” *Physical review letters* **96**, 058102 (2006).
- [43] G. De Canio, E. Lauga, and R. E. Goldstein, “Spontaneous oscillations of elastic filaments induced by molecular motors,” *J R Soc Interface* **14** (2017), 10.1098/rsif.2017.0491.
- [44] P. Baconnier, D. Shohat, C. Hernández López, C. Coulais, V. Démery, G. Düring, and O. Dauchot, “Selective and collective actuation in active solids,” *Nature Physics* **18**, 1234–1239 (2022).
- [45] Martin Brandenbourger, Colin Scheibner, Jonas Veenstra, Vincenzo Vitelli, and Corentin Coulais, “Active impact and locomotion in robotic matter with nonlinear work cycles,” arXiv:2108.08837 (2021).
- [46] David L. Christensen, Srinivasan A. Suresh, Katie Hahm, and Mark R. Cutkosky, “Let’s All Pull Together: Principles for Sharing Large Loads in Microrobot Teams,” *IEEE Robotics and Automation Letters* **1**, 1089–1096 (2016).
- [47] The precise number of particles  $N$ , which does not affect the bifurcation phenomena, was chosen because of experimental considerations such as manufacturing and visualization. In addition, we also ran an additional experiment  $N = 17$ , which displays the same self-oscillating pattern (see SI). Finally, we performed a linear stability analysis in the SI, which also demonstrates that the unstable mode does not depend on system size.
- [48] F. Bosi, D. Misseroni, F. Dal Corso, S. Neukirch, and D. Bigoni, “Asymptotic self-restabilization of a continuous elastic structure,” *Physical Review E* **94**, 1–10 (2016).
- [49] Peter Hagedorn, “on the Destabilizing Effect of Non-Linear Damping in Non-Conservative Systems With Follower Forces,” **5**, 341–358 (1970).
- [50] Davide Bigoni and Giovanni Noselli, “Experimental evidence of flutter and divergence instabilities induced by dry friction,” *Journal of the Mechanics and Physics of Solids* **59**, 2208–2226 (2011).
- [51] H. Ziegler, “Die Stabilitätskriterien der Elastomechanik,” *Ingenieur-Archiv* **20**, 49–56 (1952).
- [52] Zeno Farkas, Imre Derényi, and Tomas Vicsek, “Dynamics of Actin Filaments in Motility Assays,” *Structure and Dynamics of Confined Polymers*, 327–332 (2002).
- [53] Rolf E. Isele-Holder, Jens Elgeti, and Gerhard Gompper,

- “Self-propelled worm-like filaments: spontaneous spiral formation, structure, and dynamics,” *Soft Matter* **11**, 7181–7190 (2015), arXiv:1508.01418.
- [54] Roland G. Winkler, Jens Elgeti, and Gerhard Gompper, “Active polymers — Emergent conformational and dynamical properties: A brief review,” *Journal of the Physical Society of Japan* **86**, 1–14 (2017).
- [55] Ken Sekimoto, Naoki Mori, Katsuhisa Tawada, and Yoko Y. Toyoshima, “Symmetry breaking instabilities of an in vitro biological system,” *Physical Review Letters* **75**, 172–175 (1995).
- [56] A more accurate description would include additional effects such as noise in the active force and anisotropic viscous drag. In the former case, the noise is multiplicative in the equations of motion, which in turn progressively introduces noise to the trajectory of the active chain as the noise of the active force is increased, See SI.
- [57] See Supplemental Material [url] for simulations and theory, which includes Refs. [35, 38, 43, 55, 64, 65].
- [58] Chien-Jung Lo, Yoshiyuki Sowa, Teuta Pilizota, and Richard M Berry, “Mechanism and kinetics of a sodium-driven bacterial flagellar motor,” *Proceedings of the National Academy of Sciences* **110**, E2544–E2551 (2013).
- [59] S Gonzalez and R Soto, “Active colloidal chains with cilia-and flagella-like motion,” *New Journal of Physics* **20**, 053014 (2018).
- [60] We find that the model overestimates the magnitude of oscillations by a factor 2 and that it fails to capture the decrease of self-snapping frequency as the chains is more compressed. We attribute the discrepancy between the experiment and the model to the fact we assumed the friction to be isotropic. In reality, the lateral drag is much larger than the longitudinal drag and this simplifying hypothesis can plausibly lead to predictions that overestimate the magnitude and the frequency of snapping.
- [61] For the experimental results, the dip in the frequency miss-match at intermediate stiffness is due to friction effect that could not be avoided for small beam stiffness.
- [62] Arkady Pikovsky, Michael Rosenblum, and Jürgen Kurths, “Synchronization: a universal concept in nonlinear science,” (2002).
- [63] Corentin Coulais, Romain Fleury, and Jasper van Wezel, “Topology and broken hermiticity,” *Nature Physics* **17**, 9–13 (2020).
- [64] Warren Clarence Young, Richard Gordon Budynas, Ali M Sadegh, *et al.*, *Roark’s formulas for stress and strain*, Vol. 7 (McGraw-Hill New York, 2002).
- [65] J. Guckenheimer and P. Holmes, *Nonlinear Oscillations, Dynamical Systems, and Bifurcations of Vector Fields*, Applied Mathematical Sciences (Springer, 1983).